Design and Analysis of an Overshot Water Wheel for a Grid-Connected Pico-Hydro System

Victor Bogo Polidorio

Supervised by:

Prof. Dr. Américo Vicente Teixeira Leite

Prof. Dr. Ednei Luiz Miotto

Bragança

2019-2020

Design and Analysis of an Overshot Water Wheel for a Grid-Connected Pico-Hydro System

Victor Bogo Polidorio

Thesis presented in the School of Technology and Management of the Polytechnic Institute of Bragança to fulfill the requirements of a Master of Science Degree in Industrial Engineering (Electrical Engineering branch), in the scope of the Double Degree Program with the Federal University of Technology - Paraná

Supervised by:

Prof. Dr. Américo Vicente Teixeira Leite

Prof. Dr. Ednei Luiz Miotto

Bragança

2019-2020

Acknowledgements

Abstract

The increase in energy demand, accompanied by the concern to reduce environmental impacts, has intensified the research and use of renewable energy sources. In this context, pico-hydro systems have been intensively investigated due to being environmentally sustainable and for their potential in complementing distributed generation systems and microgrids. Within this class of power generation, water wheels are a prominent choice in sites with low heads and flowrates. Although they may seem a rudimentary solution for the present scenario, in the last two decades, they have returned to the interest of the scientific community and can be an effective alternative for generating clean energy in rural and remote areas without access to the conventional power grid. In urban centres with a well-established power grid, water wheels, such as photovoltaic systems, can contribute to meeting the ever-increasing demand for electricity. One of the main challenges for this technology dissemination lies in the fact that the design of the system depends on the characteristics of the place where it will be installed and, usually, it is done in such a way that the water wheel operates in a very narrow speed range. In this context, this work presents the design and mathematical modelling of an *overshot* water wheel, as well as the application of theoretical models to estimate its efficiency, aiming to identify its behaviour within an operational range. From the results, the design of a grid-connected pico-hydro system was made, based on permanent magnet synchronous generators and conventional photovoltaic micro-inverters, allowing the water wheel to operate at variable speed. Additionally, the integration with the grid using conventional photovoltaic micro-inverters, as presented in this work, can facilitate the dissemination of these systems, as they are a mature and ready-to-use technology.

Keywords: pico-hydro systems; water wheels; grid connection; renewable energy

Resumo

O aumento da demanda energética, acompanhado da preocupação em reduzir os impactos ambientais, intensificou a pesquisa e o uso de fontes de energias renováveis. Nesse contexto, os sistemas pico-hídricos têm sido intensamente investigados por serem ambientalmente sustentáveis e pelo seu potencial em complementar sistemas de geração distribuída e microrredes. Nessa classe de geração de energia, as rodas d'água são uma escolha proeminente em locais com baixas quedas e caudais. Embora possam parecer uma solução rudimentar para o cenário atual, nas últimas duas décadas elas voltaram ao interesse da comunidade científica, podendo ser uma alternativa eficaz para geração de energia limpa em áreas rurais e remotas sem acesso à rede elétrica convencional. Em centros urbanos com a rede elétrica bem estabelecida, tal como os sistemas fotovoltaicos, as rodas d'água podem contribuir para o atendimento da crescente demanda por energia elétrica. Um dos principais desafios para a sua disseminação está no fato de que o projeto do sistema depende das características do local onde será instalado e, normalmente, é feito de forma que a roda d'água opere em uma faixa de velocidade muito estreita. Neste contexto, este trabalho apresenta o projeto e modelagem matemática de uma roda d'água *overshot*, bem como a aplicação de modelos teóricos para estimar sua eficiência, visando identificar seu comportamento dentro de uma faixa operacional. A partir dos resultados, o projeto de um sistema pico-hídrico conectado à rede foi realizado, baseado em geradores síncronos de ímãs permanentes e micro inversores fotovoltaicos convencionais, permitindo que a roda d'água opere em velocidade variável. Além disso, a integração com a rede utilizando esta tecnologia, como apresentada nesse trabalho, pode facilitar a disseminação desses sistemas, por serem uma tecnologia madura e pronta para uso.

Palavras-chaves: sistemas pico-hídricos; rodas d'água; conexão à rede; energias renováveis

Contents

List of Tables

List of Figures

Acronyms

AC   Alternate current

DC   Direct current

DG   Distributed generation

ESTiG   Escola Superior de Tecnologia e Gestão

ICNF   Institute for Nature and Forest Conservation

IEA   International Energy Agency

IPB   Instituto Politécnico de Bragança

LHP   Large Hydropower

MPPT   Maximum power point tracking

PM   Permanent magnet

PMSG   Permanent magnet synchronous generator

PV   Photovoltaic

SHP   Small Hydropower

Symbols

D Diameter [m]

H Head [m]

H_{gr} Gross head [m]

H_{net} Net head [m]

I Electrical current [A]

L Power loss [W]

N Rotational speed [rpm]

N_{cr} Critical rotational speed [rpm]

P Active power [W]

P_{gr} Gross power [W]

P_{net} Net power [W]

Q Flow rate [m^3/s]

R Radius [m]

R_i Inner radius [m]

R_o Outer radius [m]

$\mathbf{V}$ Voltage [V]

V Volume [m^3]

c Relative flow speed [m/s]

d Bucket depth [m]

f Frequency [Hz, s^{-1}]

g Gravitational acceleration [m/s^2]

h_o Horizontal length of water surface [m]

n Number of buckets [rpm]

n_m Rotor speed [rpm]

p Number of poles [-]

u Wheel tangential speed [m/s]

v Flow speed [m/s]

w Wheel width [m]

α Water surface inclination [rad, degree]

β Angle between two blades/buckets [rad, degree]

γ Specific weight [N/m^3]

η Efficiency [-]

θ Angular position [rad, degree]

ξ Impact coefficient [-]

ρ Density [kg/m^3]

ω Angular speed [rad/s]

Chapter 1

Introduction

The increase in energy demand, coupled with the growing concern about the use of fossil fuels and their environmental impacts, has mobilized different groups around the theme. The International Energy Agency (IEA) anticipates an increase of more than 25% in the global primary energy demand between 2017 and 2040 in a scenario in which energy efficiency improvements occur [1]. Without these improvements, the demand rise is projected to be twice as large. Furthermore, electricity demand is expected to grow by 60% [1]. At the same time, there is a concern to reduce or at least limit fossil fuels' consumption and the emission of greenhouse gases. To this end, several goals have been set to promote improvements in energy efficiency and the long-term transition to an energy model based on renewable sources, such as the directives established in the legislation of the European Commission [2], [3] and those indicated by the United Nations 2030 Agenda for Sustainable Development [4]. Consequently, there is a great interest in wind, solar, and hydropower.

Figure 1.1 shows the generation of electricity by source between 1990 and 2019. It is possible to observe an expansion of the electricity share generated by renewable sources, defined mainly by the high hydroelectric contribution and the rapid growth of wind and solar power. Despite this, individually, coal remained the largest power generation source, and fossil fuels remained the dominant source

of total production, as shown in Figure 1.2. Therefore, renewable energy sources must have an even more significant growth to meet sustainable development goals.

Electricity Generation by Source, World
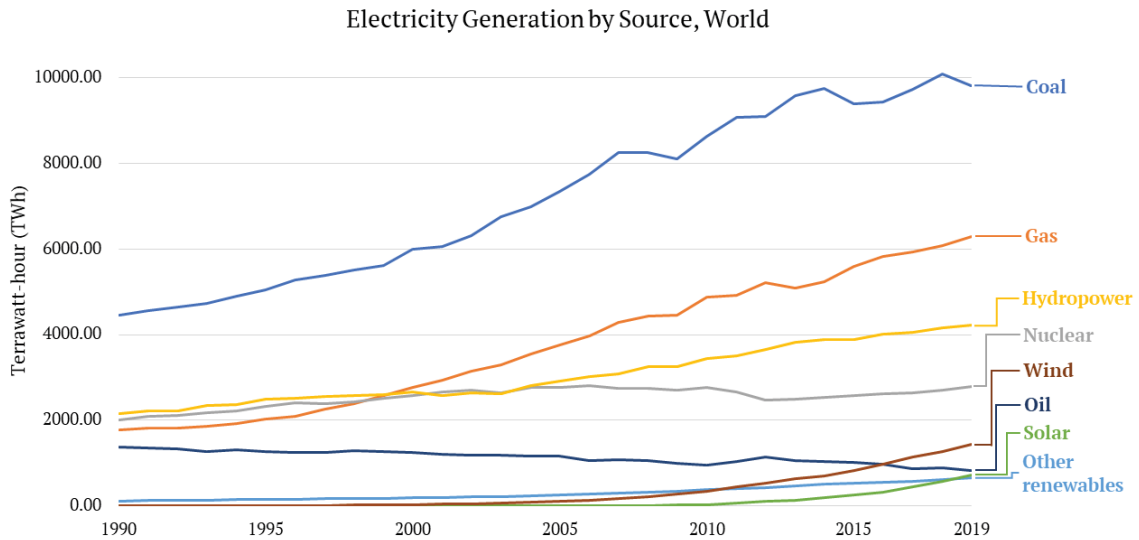
Figure 1.1 Electricity generation by source, 1990-2019 [5]. Note: 'Other renewables' includes biomass, waste, geothermal, and wave and tidal energy.
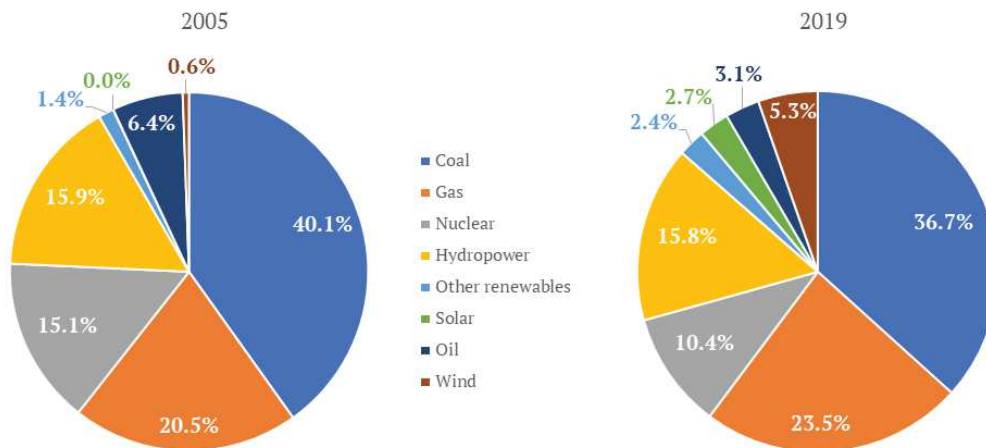
Figure 1.2 Comparison of electricity generation by source, 2005 and 2019 [5].

Hydropower is a well-established technology, and compared to other clean energy sources, such as wind and solar, it has reached a high level of technological maturity. Additionally, hydroelectric plants have a wide range of variability in scale, with stations of a few kilowatts (kW) of power capacity to stations with several gigawatts (GW) of power capacity. Although the principles between plants

of different scales may be similar or even identical, the technological and market maturity is not the same [6], [7]. Furthermore, the development of large-scale hydropower plants has a considerable environmental impact, mainly in dams construction. Small-scale hydropower plants do not have such an environmental impact, as they are usually systems without or with shallow reservoirs [8], [9].

Small-scale hydropower systems play a significant role in complementing distributed generation systems and microgrids [8], [10]. They are especially relevant for providing clean energy to rural communities and remote areas without access to the grid, especially in developing countries [9], [11]. Besides, in the field of micro-hydropower, there is untapped potential with low-head differences (a few meters) available in rivers, irrigation channels, and old mill sites [10]. However, existing technologies for such scales are not always cost-effective, preventing these systems' widespread exploitation.

In this context, recent advances in pico-hydro power converters have improved their cost-effectiveness. Gravity water wheels, in particular, have been extensively tested in scientific projects [12], [13]. In addition to their environmental impacts, especially on fish populations, being minimal, their typical values of global efficiency ranges from 50 to 70%. Furthermore, water wheels are advantageous when using existing civil structures, such as old water mills [14], becoming educational, tourist, and recreational sites.

1.1 Contextualization

In the Polytechnic Institute of Bragança (IPB), several investigations and implementation projects related to pico-hydro systems using permanent magnet synchronous generators as a way to exploit the energy available in rivers and watercourses have been carried out [14]–[20]. In this context and within the scope of the BIOURB NATUR Project – *Bio constructive diversity, bioclimatic buildings, sustainable rehabilitation and its application in natural spaces* – an

energy solution is being developed to transform the Castrelos' Aquaculture Center into a self-sustainable building, through the integration of different energy generation systems based on renewable sources, namely photovoltaic and pico-hydropower, in a smart micro-grid [19]. The pico-hydro generation system was designed in a laboratory of the School of Technology and Management (ESTiG), at IPB, and includes an overshot water wheel, which will serve as the basis for the system to be designed and analyzed in the present work.

The BIOURB NATUR project is developed in collaboration between the IPB and the Institute for Nature and Forest Conservation (ICNF) [19]. The Castrelos' Aquaculture Center produces trout for the repopulation of watercourses in the region of Bragança, Portugal. Additionally, recently it has been a space for the development of actions to promote environmental awareness and education for the public [19].

1.2 Objectives

The main objective is to design an overshot water wheel, in the context of a grid-connected pico-hydropower system.

Specific objectives include:

- The design and mathematical modelling of an overshot water wheel;

- Apply theoretical models to estimate the efficiency of the water wheel, and identify its behavior within an operational range;

- Design the energy conversion systems identifying the electrical generator suitable for the application and the system's interface with the grid, through a theoretical analysis.

1.3 Thesis structure

- Chapter 1: Presents an introduction and the objectives of this work;

- Chapter 2: Contains an explanation and review of theoretical concepts related to the hydropower generation, focusing on pico-hydro systems;

- Chapter 3: Presents the design criteria and theoretical model to estimate the efficiency of overshot water wheels;

- Chapter 4: Presents the developed mathematical modelling of the investigated water wheel and its design;

- Chapter 5: Contains the theoretical results and its analysis;

- Chapter 6: Presents the conclusion, as well as suggestions for future works.

Chapter 2

Theoretical Background

This chapter presents an explanation and review of theoretical concepts referenced throughout the thesis, such as the fundamentals of hydraulic energy conversion systems, types of hydraulic turbines, electric generators, distributed generation, and the integration between pico-hydropower systems and the grid.

2.1 Hydroelectricity

Hydropower generation has an essential role in the world energy matrix, contributing to 60% of the electricity generated among all renewable sources and providing 15.8% of the world's electricity generated from all sources [5].

Hydropower plants are, generally, classified by size, i.e., their production capacity. Although there is no agreed definition, the United Nations Industrial Development Organization (UNIDO) distinguish two principal categories: *large* for production capacity over 10 MW and *small* for production capacity under 10 MW [11]; additionally, the International Renewable Energy Agency (IRENA), presents the following classifications: *mini* for production capacity under 1 MW; *micro* for production capacity under 100 kW and *pico* for production capacity under 5 kW [21]. Most of the world's hydropower installed capacity refers to Large Hydropower (LHP), where Small Hydropower (SHP) represents only 7.5% of the

total hydropower capacity. However, it is estimated that 66% of the world's SHP potential remains untapped [11].

2.1.1 Power from water

Hydropower generation works on the principle of moving water, being directly dependent on the flow of water and a drop in height, also referred to as a 'head' (vertical difference between the upstream water level and the downstream water level) [22]. The available power is:

$$P_{gr} = \rho g Q H_{gr} \tag{2.1}$$

where P_{gr} is the gross power (W), ρ is the density of water (kg/m^3), g is the gravitational acceleration (m/s^2), Q is the flow rate (m^3/s), and H_{gr} is the gross head (m).

A hydropower plant is a power conversion system that absorbs power in the form of head and flow and provides electricity or mechanical shaft power. However, no power conversion system can deliver as much usable power as it absorbs, presenting losses in the form of friction, heat, noise, and others. Therefore, the overall efficiency of a hydropower plant can be defined as:

$$\eta = \frac{P_{net}}{P_{gr}} \tag{2.2}$$

where η is the overall efficiency and P_{net} is the net power (the power usefully delivered) (W).

2.2 Small-hydro generation

Small-hydro generation has been an effective alternative for providing access to clean and sustainable electricity worldwide, especially in rural and remote areas without access to the grid. SHP also helps developed countries achieve targets for advancing renewable energy and reducing greenhouse gas emissions [11]. In this aspect, mini, micro, and pico hydropower are increasingly proving to be reliable

energy sources. Besides being more environmentally sustainable and having short payback periods than LHP plants, suitable sites are available in almost every part of the world [9], [23].

Micro and pico hydropower plants are almost always run-of-river systems, which means that they do not stop the river flow. Instead, it diverts part of the flow into a channel and pipe and then through a turbine. This type of system can be built locally at a low cost, and its simplicity gives rise to better long-term reliability. Additionally, run-of-river plants are more environmentally friendly since the river flow downstream of the installation is not affected, and there is no need for the building of large dams [22]. Another advantage of these systems is their low daily variability, which makes it able to produce energy all day, except in long periods of drought. Moreover, recent studies have facilitated pico-hydro systems' connection with the grid, using conventional wind and photovoltaic (PV) inverters and low-speed generators [16], [18].

2.3 Turbines

Turbines are machines that extract energy from fluids in the form of work or power. In hydraulic turbines, the working fluid is water. In a turbine, a stage typically consists of an element to accelerate the flow, converting some of its pressure energy to kinetic energy, followed by a rotor, wheel, or runner that extracts the kinetic energy from the flow [24]. To choose the optimal turbine for a specific site, a careful analysis of the head and the flow rate available must be done [25]. Figure 2.1 shows the operating conditions of hydraulic turbines. The two most general classifications of turbines are impulse and reaction turbines [24].
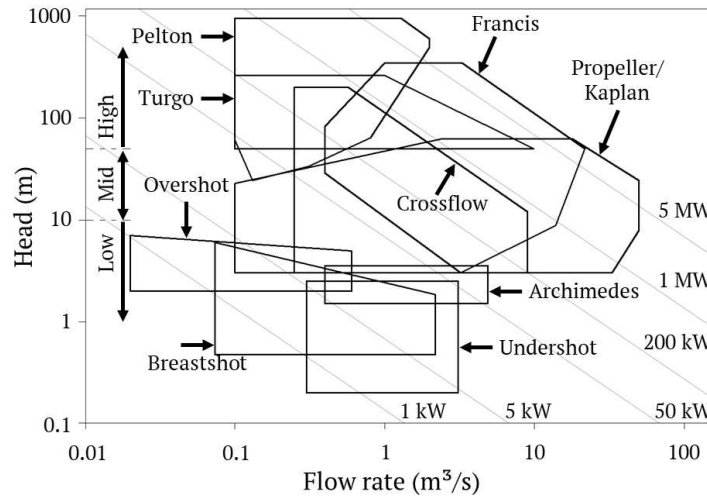
Figure 2.1 Operating conditions of hydraulic turbines [26].

In reaction turbines, the rotor is enclosed in a pressure casing and fully immersed in water. The runner blades are designed to exploit the lifting force that occurs due to the pressure difference between them, which causes the runner to rotate. In the late nineteenth and early twentieth centuries, reaction turbines began to be employed as micro and mini hydropower converters in sites with heads below 2,5 m [27]. The most used reaction turbines are Kaplan and Francis [23], illustrated in Figure 2.2.
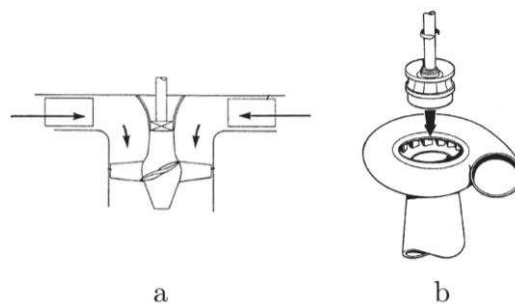
Figure 2.2 Reaction turbines: (a) Kaplan, and (b) Francis [22], [28].

In contrast with reaction turbines, the runner of impulse turbines operates in air at atmospheric pressure. A water jet moves the rotor blades without pressure differences across it [23]. Generally, impulse turbines operate better in medium and high heads, above 10 meters [26]. The main types of impulse turbines

are Pelton, Turgo, and Crossflow. Stream water wheels also fall into this classification [12]. Figure 2.3 shows the turbines mentioned previously.
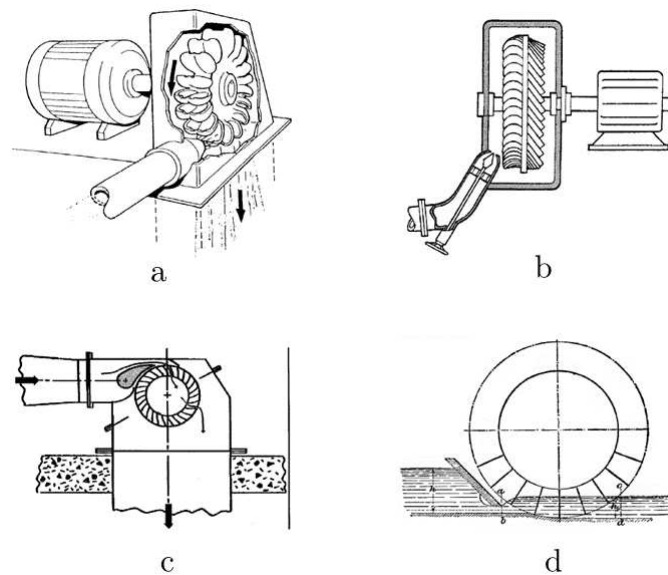
Figure 2.3 Impulse turbines: (a) Pelton, (b) Turgo, (c) Crossflow, and (d) Stream water wheel [28], [29].

In addition to these traditional hydraulic machines, another classification that has been the subject of recent studies are the gravity turbines, which exploit the hydrostatic force of water and operate in open-air [12], [23], [25]. The most common types of gravity turbines are the Archimedes screw and gravity water wheels.

The Archimedes screw is one of the oldest known hydraulic machines. Initially, it was employed as a pump, but its potential as a hydropower converter was identified in the early 19th century. However, its first tests as a hydropower machine were reported only recently [27]. The Archimedes screw rotates around an inclined axle at 22° to 35° from the horizontal [23]. When the outer tube does not rotate with the screw, acting only as a support, it is instead called a hydrodynamic screw [12]. Figure 2.4 shows an Archimedes screw.
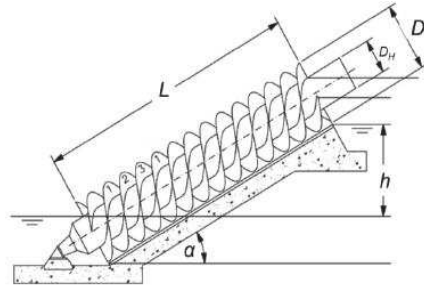
Figure 2.4 Archimedes screw [27].

Gravity water wheels rotate around a horizontal axle. They can be divided into three main types: overshot, where the water enters from the top of the wheel, breastshot where the entry point of the water is near or at the level of the wheel axle, and undershot in which the water enters the wheel below it axle [13], [29], [30]. Water wheels will be further described in the next section.

2.3.1 Water wheels

Water wheels have been known since antiquity and were primarily used as a power source for grinding grains [31]. They can be divided into horizontal and vertical wheels.

Horizontal wheels have a vertical rotational axle and are considered impulse wheels. Figure 2.5 illustrates a horizontal water wheel. The impact of the water on its blades causes the wheel to rotate. Usually, horizontal water wheels are smaller and have a higher rotational speed than vertical water wheels [23]. Their maximum hydraulic efficiency is around 50% [32].
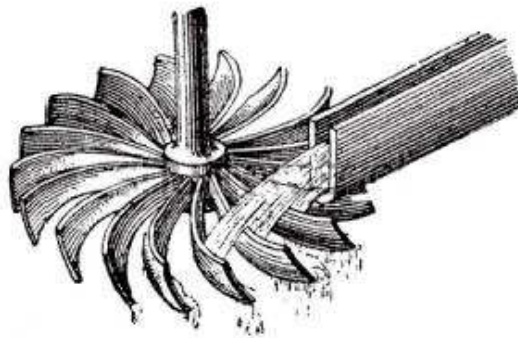
Figure 2.5 Horizontal water wheel [23].

On the other hand, vertical wheels have a horizontal rotational axle and can be further classified into stream and gravity wheels. Gravity wheels are potential energy converters, operating almost entirely by gravity (i.e., by the weight of the water). Instead, stream wheels are kinetic energy converters, working purely by the kinetic energy of moving water [23], [29], [33].

Stream wheels are hydrokinetic machines, where the effect of the water weight is negligible. This type of wheel utilizes the kinetic energy of a stream. If a head of water is available, the entirety of the head's potential energy is converted into kinetic energy before coming in contact with the wheel [23], [29]. They are used in sites with shallow heads or flowing water [34].

Gravity water wheels are used in sites with higher heads, as they mainly exploit the potential energy of water. As described before, there are three main types of gravity water wheels: overshot, breastshot, and undershot. Furthermore, breastshot water wheels can be divided into high, middle, and low, according to the wheel's water entry point, being low breastshot equivalent to undershot water wheels [12], [13], [30]. Figure 2.6 depicts these types of water wheels.
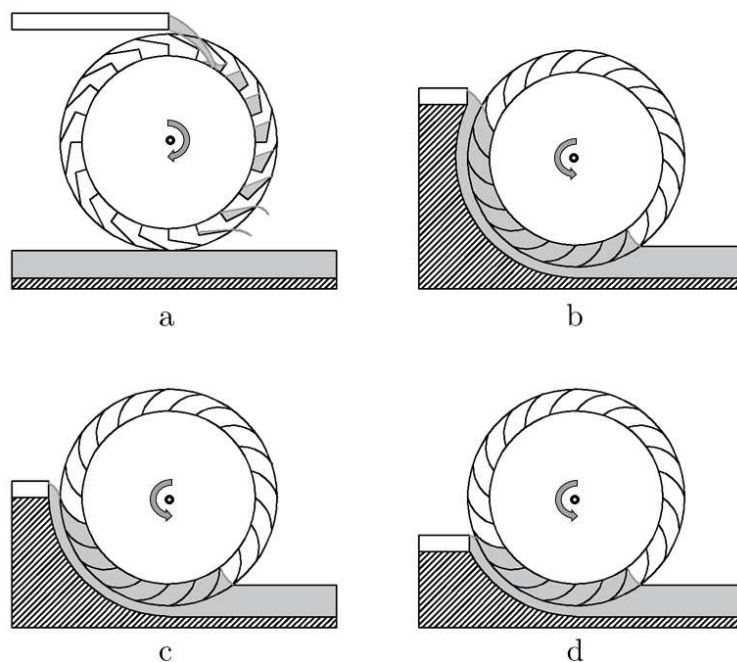
Figure 2.6 Gravity water wheel types: (a) overshot, (b) high breastshot, (c) middle breastshot, and (d) low breastshot/undershot. Adapted from [23].

In overshot water wheels, the water enters from the top of the wheel. They are generally employed for head differences between 2.5 m and 10 m and flow rates between 0.1 m³/s and 0.2 m³/s per meter width [13], [35]. Overshot water wheels' maximum efficiency was identified in the range of 80–85% [12].

Breastshot water wheels receive the water from the upstream side of the wheel. Additionally, they rotate in the opposite direction of traditional overshot wheels [12], [36]. They are mostly employed for head differences between 1.5 m and 4 m and flow rates between 0.35 m³/s and 0.65 m³/s per meter width. Their maximum efficiency ranges between 75% to 85% [12], [13].

Similarly to the breastshot, undershot water wheels receive the water from their upstream side, being different at the water entry point. As there is no precise rule that makes this differentiation, it is conventional to assume that undershot wheels have the water entry point in their lowest third portion [12]. They are used for head differences between 0.5 m and 2.5 m and flow rates ranging from 0.5 m³/s up to 1 m³/s per meter width [12], [13]. As well as the breastshot, the maximum efficiency of undershot wheels is between 75% and 85% [12].

2.4 Electric Generators

An electrical generator is an electrical machine used to convert mechanical energy from an external source, such as a turbine shaft, into electrical power. They can be classified into direct current (DC) generators and alternate current (AC) generators. Furthermore, AC generators can be divided into synchronous and asynchronous (or induction) generators. The choice of a generator for a specific application depends on several factors, such as the prime mover speed, the required output power, range of operation, and end-use (e.g., grid connection or battery charging) [37]. In SHP, the most used generators are the synchronous, mainly the permanent magnet synchronous generator (PMSG), and the induction

generator [37]–[39]. DC generators are not usually used because they require frequent maintenance and are more expensive than AC generators.

2.4.1 Induction Machines

In induction machines, an electric field is induced by a relative movement (slip) between the rotor and the stator's rotating field, which produces a voltage across the rotor winding. The rotor's magnetic field interaction with the stator field results in the torque on the rotor [40].

The rotor of induction machines can be divided into two types: squirrel-cage rotor and wound-rotor. In a wound-rotor machine, the rotor winding terminals are connected to insulated slip rings mounted on the machine shaft. Carbon brushes bearing on these rings make the rotor terminals available externally to the machine [41]. In squirrel-cage rotor machines, the winding consists of conductive bars embedded in slots in the rotor iron and shorted-circuited at each end by conducting end rings. Squirrel-cage rotor machines are more robust and have a low maintenance requirement, unlike wound-rotor machines [41].

For an induction machine to operate as a generator, it is necessary to provide mechanical power from a primary machine (turbine) that must accelerate the rotor to a speed higher than the synchronous speed. Additionally, it must be supplied with reactive power capable of exciting the air gap magnetic field [41]. In on-grid operation, the reactive power can be obtained directly from the grid. However, in the off-grid mode, it is necessary to use capacitor banks [40].

In the pico-hydro generation, squirrel-cage induction generators are an attractive option for capacity over 1 kW due to their low cost and robustness. However, they are designed to operate in a very narrow speed range [37], [38]. Another disadvantage is the need for capacitor banks for off-grid operation, making it more suitable for on-grid applications [42].

2.4.2 Synchronous Generators

A synchronous machine is one in which alternating current flows in the armature winding and a rotor DC flux is produced, either by a DC excitation supplied to the field winding or by permanent magnets that replace the field windings on the machine rotor. The excitation system provides the DC power required for the machine excitation. In the case of a synchronous machine with permanent magnets, there is no need for an external source to excite the rotor's DC flux [41].

In synchronous generators, the electrical frequency of the energy produced is related to the rotor's speed and the number of poles of the machine according to the following equation [43]:

$$f_e = \frac{n_m P}{120} \tag{2.3}$$

where f_e is the electrical frequency (Hz), n_m is the rotor speed (equals to the magnetic field speed in synchronous machines) (rpm), and P is the number of poles [43].

Permanent Magnet Synchronous Generator

Permanent magnet (PM) AC generators are polyphase synchronous generators in which permanent magnets replace the field windings. Additionally, they do not require slip rings and brushes [41].

Regarding pico-hydropower, PMSG are more suitable for off-grid applications than induction generators, as they do not need to be supplied with reactive power (either from the main grid or capacitor banks) to produce the magnetic field [42]. Furthermore, in on-grid applications, when the grid connection of PMSG is made using a power converter, pico-hydropower plants can work at variable speed, allowing the system (converter's control algorithm) to maximize the energy production [18], [38], [44].

2.5 Distributed Generation

Most of the electricity produced in the world is generated in large generating stations. These stations produce and transmit electricity through high-voltage transmission systems and then, at reduced voltage, transmit it through the local distribution systems to consumers. However, the electricity can also be produced by distributed generation (DG) plants. In contrast with large generating stations, they produce power on a customer's site or at a local distribution utility. Some or all the power is consumed, and any surplus is sent directly to the local distribution grid. DG technologies include engines, small turbines, fuel cells, photovoltaic systems, and others. Although they represent a small share of the electricity market, DG technologies already play a crucial role and can fundamentally alter the electric power system's structure and organization [45].

In the literature, however, there is no consensus on the definition of DG. Many terms refer to this type of generation, such as: 'embedded generation' for Anglo-American countries, 'dispersed generation' for North American countries, and 'decentralized generation' in Europe and Asia [46], [47].

The International Council on Large Electric Systems (CIGRE) defines DG as all generation units with a maximum capacity smaller than 50-100 MW, usually connected to the distribution grid and which are neither centrally planned nor dispatched [47], [48]. On the other hand, the Institute of Electrical and Electronics Engineers (IEEE) defines DG as the generation of electricity by facilities sufficiently smaller than central generating plants to allow interconnection at nearly any point in a power system [47], [48].

In general, DG is a source of electric power generation or storage that is not a part of a large central power system and is located close to the load. They can be categorized as renewable and non-renewable and can either be grid-connected or operate independently of the grid [45], [48].

2.5.1 Isolated and Grid-connected Systems

DG systems can operate in two different modes, grid-connected or isolated. Grid-connected systems, also known as on-grid systems, are connected to the utility grid. They can feed any excess generated power into the grid and draw power from it when the generation is lower than the demand.

For a DG system to operate in on-grid mode, certain restrictions and requirements should be met, such as functioning at the main grid's frequency and voltage. Therefore, devices enabling the synchronization between on-grid systems and the utility grid are required in such configuration [49].

Isolated systems, also known as stand-alone, islanded, or off-grid systems, are generation units disconnected from the primary power grid. They are more suitable for remote regions where the utility grid is not available. They are often applied to rural electrification, lighthouses, auxiliary power units for emergency services, military applications, or water pumping [50], [51]. Furthermore, in recent years these systems have been integrated into smart microgrids at the urban level, such as in residences and public and commercial buildings [15], [52]. Usually, this type of system has some type of energy storage to store the excess power produced, especially during off-peak demand periods [51].

2.6 Grid Connection of Pico-Hydro Systems

As mentioned in section 2.5, distributed generation systems can operate connected or isolated from the utility grid. In off-grid operating conditions, it is essential to provide effective regulation of the voltage and frequency to suit these systems to the connected appliances. Additionally, in on-grid systems, besides the voltage and frequency regulation, the synchronization with the grid also needs to be considered [16]–[18].

Pico-hydro power plants are frequently used as stand-alone systems, with a turbine driving a generator. The regulation of the output voltage and frequency

is made using a load controller [50]. When operating connected to the utility grid, the conventional pico-hydro systems are designed to work at a very narrow speed range, so the rotational speed is as close as possible to the generator's rated speed [18], [53].

Recent studies address the integration between the grid and pico-hydropower systems using PMSG and PV inverters [16]–[18], which allows the system to operate at variable speed, and consequently, different hydraulic conditions (head and flow). Furthermore, PV inverters are mature and ready-to-use technology. For proper operation and safety, the system also requires an overvoltage protection circuit. Figure 2.7 illustrates this topology.
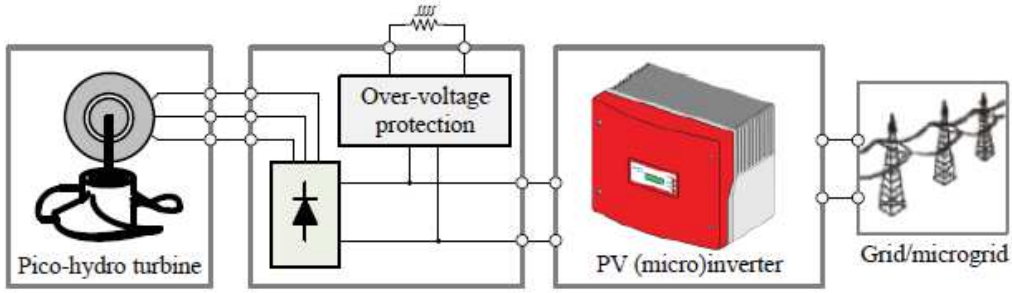
Figure 2.7 Topology of grid-connected pico-hydro systems using PV inverter [16].

The integration procedure is done by overlapping the operating areas of the PV inverter and the generator, as shown in Figure 2.8, and the following conditions must be guaranteed [16]:

- The rated power of the generator must be in the range of $0.4P_{DC\max}$ and $P_{DC\max}$ of the inverter, being $P_{DC\max}$ its maximum input power;

- The rectified output voltage of the generator ($\mathbf{V}_{DC}$) should be within the input voltage range of the PV inverter;

- The rectified current (I_{DC}) of the generator should not exceed the maximum input current ($I_{DC\max}$) of the inverter;

19

- The maximum DC voltage allowed by the overvoltage protection circuit should be lower than the maximum input voltage ($\mathbf{V}_{DC\max}$) of the inverter;

- The no-load DC voltage of the generator for the initial speed must be higher than the minimum input voltage needed for the invert to start working ($\mathbf{V}_{PVstart}$).

Moreover, the system dynamics must be compatible with the maximum power point tracking (MPPT) algorithm of the PV inverter.
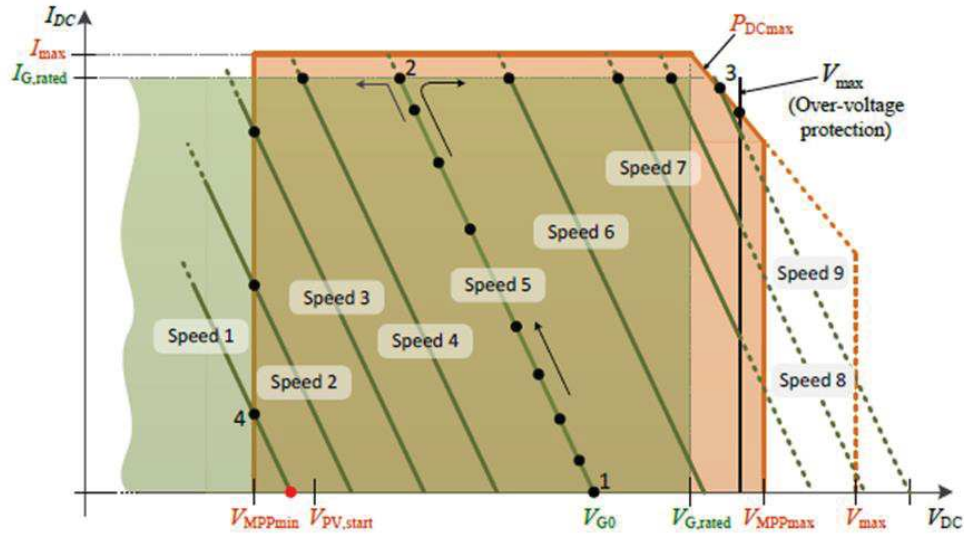
Figure 2.8 Overlapping of the operation areas of the PV inverter and the generator [16].

Considering that the conditions, as mentioned earlier, are met, Figure 2.8 (black dots) shows a possible path of operation for the PMSG, set by the inverter's MPPT algorithm. For an initial speed, "Speed 5", the MPPT algorithm will start from point 1 and increases the generators current up to its maximum value (point 2). From this point, if the speed increases up to "Speed 9", the operating point will be set in point 3, given that the corresponding voltage is lower than the maximum voltage allowed by the over-voltage protection. However, from point 2, if the generators speed decreases to "Speed 1", the operating point will be set in point 4 [16].

Chapter 3

Theory Behind an Overshot Water Wheel

This chapter presents the theoretical concepts used in the design of overshot water wheels and the theoretical model to estimate its power losses.

3.1 Design of an overshot water wheel

Water wheels are designed for a given application, head difference, and water flow. For an overshot water wheel, the diameter is determined by the head difference [13]. In the historical literature, they have been designed with a diameter slightly smaller than the distance between the upstream channel bed and the downstream water surface. A practical rule that can be used is $D = 0.85H$, where D is the wheel diameter, and H is the head [23].

According to [12], the number of buckets (or blades), n, generally ranges between 20 and 50, and an applicable rule can be $n = 16R$, where R is the wheel radius in meters (m). It is also shown in [12] that existent installed overshot water wheels have their number of buckets similar to those described by the literature, with an interpolating equation equals to $n = 14.8R + 6.3$. The bucket depth

(the length of the cell along the radial direction) d is generally between 0.2 m and 0.35 m [12].

Ideally, the overshot water wheel's cells must hold the water until the wheel's lowest position, where it then empties rapidly. To avoid an early loss of water each bucket should only be filled with 30% to 50% of its maximum volume [13], meaning a filling ratio (water volume inside the bucket to the total volume of the bucket) of 0.3-0.5 [12], [13]. Once the filling ratio is chosen and knowing the flow rate, the wheel's width can be determined to satisfy the desired ratio.

It was identified in [35] that after a certain rotational speed, called critical rotational speed N_{cr}, the power losses increase significantly, and the efficiency decrease almost linearly with the speed N. The critical rotational speed can be expressed as $N_{cr} = 31.3/\sqrt{D}$ (rpm). Furthermore, this speed corresponds to when $u/v = 0.75$, where u is the wheel tangential speed (m/s), and v the flow speed (m/s) [35].

3.2 Bucket Design

Optimally, the blade profile of an overshot water wheel should be shaped so that the water jet enters each cell at its natural angle of fall, so the impact between the water jet and the bottom of the bucket is minimal, reducing the impact losses [13].

In this work, the blade profile chosen was the one with a flat bottom, as shown in Figure 3.1 (a). This design is one of the most basic found in historical literature and was widely employed in the past [29], [30], [54]. Although more efficient shapes have been reported [13], [35], [55], they present a more complex geometry for the analyzes to be conducted and do not alter the validity of the work developed.
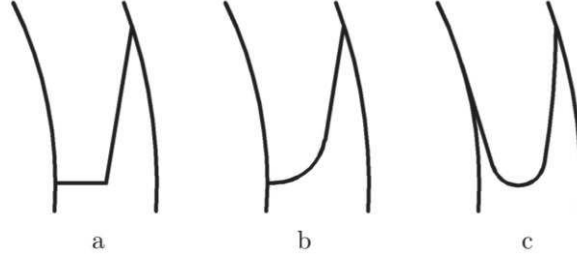
Figure 3.1 Different blade profiles: (a) flat bottom design used, (b) and (c) alternative shapes.

3.3 Efficiency Measure

3.3.1 General Theory

More than one way to estimate the losses and the efficiency of overshot water wheels were reported [29], [30], [35], [56]. The model developed by Quaranta and Revelli [35] (further described by Quaranta in [23]) is applied in the present work, as it can be considered a modern version of those described in the historical literature. In this method, the losses are calculated and subtracted from the input power, obtaining the mechanical output power and efficiency.

In the theoretical model described by Quaranta and Revelli [35], some considerations are made. The opening of each bucket is wider than the water jet so that the air can escape. It is assumed that the water inside the buckets is at rest, and the effect of the centrifugal force, which makes the profile of the water surface non-horizontal, is considered. Additionally, the contribution of the water impact in the buckets to the power generation is neglected since it is related to the kinetic energy of the water flow, which is much lower than the potential energy and does not significantly affect the results [23].

Figure 3.2 shows an overshot water wheel based on the one depicted in [35], with an internal radius R_i, an angular speed ω in rad/s, and an angular distance between two blades $\beta = 2\pi/n$ expressed in radians (rad). The angular position of each blade is θ, where $\theta = 0°$ is the vertical line that passes through the rotation axle.
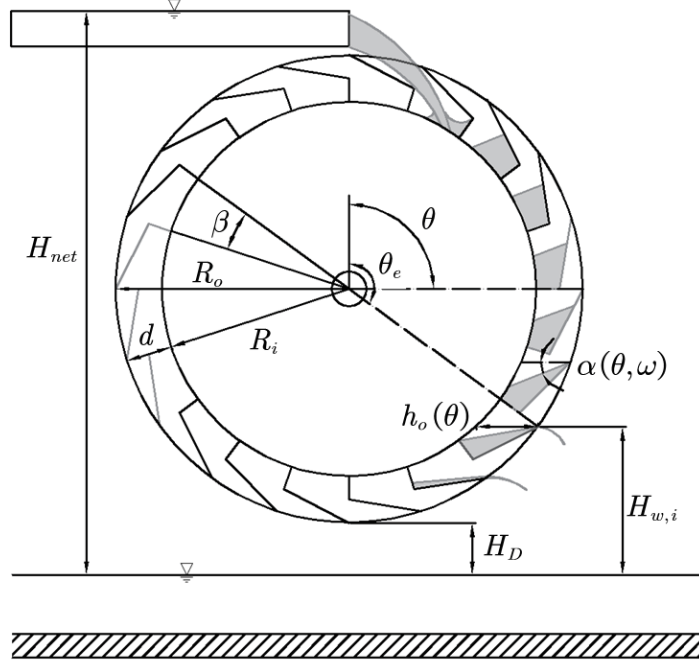
Figure 3.2 Reference scheme for the overshot water wheel, based on [35].

The hydraulic power available to the wheel is:

$$P_{net} = \gamma Q H_{net} \tag{3.1}$$

where γ is the specific weight of the water (N/m^3), Q is the flow rate (m^3/s), and H_{net} is the net head (m).

The mechanical output power P_{out} of an overshot water wheel can be expressed by [35]:

$$P_{out} = P_{net} - \sum Losses = P_{net} - L_{imp} - L_t - L_g - L_{Q_u} - L_{Q_r} \tag{3.2}$$

where L_{imp} is the loss due to the impact occurring in the inflow process, L_t the impact loss generated when the blades impact the tailrace water (if they are submerged), L_g the mechanical friction loss at the shaft, L_{Q_u} the volumetric loss at the top of the wheel, and L_{Q_r} the volumetric loss during rotation. The efficiency η is:

$$\eta = \frac{P_{out}}{P_{net}} = \frac{P_{net} - \sum Losses}{P_{net}} = 1 - \frac{\sum Losses}{P_{net}} \tag{3.3}$$

3.3.2 Power losses estimation

In this section, the power losses are described based on [35]. Whereas the wheel to be radially symmetrical, the instantaneous power losses exhibit a period of $T = \beta/\omega$ in seconds (s). To estimate the power output P_{out}, their average value during T are considered [35].

Impact Losses

Two different impact losses can be identified. One occurs at the top of the wheel and the other at the tailrace.

The impact power loss at the top of the wheel is generated when the water jet enters the buckets and can be expressed by [35]:

$$L_{imp} = \xi \gamma Q \frac{c^2}{2g} \tag{3.4}$$

where ξ is the impact coefficient and $\vec{c} = \vec{v} - \vec{u}$ is the relative velocity of the jet, being $\vec{v}$ the absolute velocity of the water jet and $\vec{u}$ the tangential velocity of the blades in the impact point. The contribution of the impact for the power generation does not significantly affect the results. For that reason, it is assumed that $\xi = 1$ [35].

The impact loss at the tailrace occurs when the blades are submerged, and their tangential speed is faster than that of the tailrace water. The loss L_t is expressible by [35]:

$$L_t = \frac{1}{2} C_D \rho (u - v_d)^2 A u \tag{3.5}$$

where v_d is the water speed at the tailrace (m/s), C_D the drag coefficient, which depends on the shape of the blade, and A is the area of the blade exposed to the impact (m²). In the present work, it is assumed that the investigated wheel is not submerged, so $L_t = 0$.

Mechanical losses

The mechanical losses are related to the friction at the shaft supports and can be expressed by [35]:

$$L_g = M\omega = WC_f r\omega = (W_{wh} + W_{wat})C_f r\omega \tag{3.6}$$

where M is the resistance torque due to the friction, and $W = W_{wh} + W_{wat}$ is the total weight, being W_{wh} the weight of the wheel, and W_{wat} the weight of the water inside the buckets, C_f is the friction coefficient and r the shaft radius. According to Quaranta [23], L_g is negligible, having the lowest values of all the losses. Therefore, in this work L_g will not be considered.

Volumetric losses

Volumetric losses occur both at the top of the wheel and during rotation.

A portion of the flowrate can be lost at the top of the wheel, generating the power loss L_{Q_u}, expressible by [35]:

$$L_{Q_u} = \gamma Q_u H_{net} \tag{3.7}$$

being Q_u the flowrate lost, which is a function of the wheel rotational speed and the blades' shape.

The complexity of the filling and impact process makes it difficult to estimate Q_u theoretically, being relative for each water wheel and its blades shapes, and depending on experimental tests. However, when water wheels are operating at their optimal performance range, i.e., at rotational speeds lower than N_{cr}, the top volumetric losses are practically zero. In this case, the theoretical model can be applied [35]. Therefore, in this work, it will be assumed that the wheel works under these conditions.

The volumetric power loss L_{Q_r} occurs when water starts to spill out from the buckets during rotation, and the bucket starts to empty. L_{Q_r} has a periodic

cycle of $T = \beta/\omega$, being β the angular distance between two blades, as shown in Figure 3.2. The instantaneous power loss at the instant $t = t_j$ is [35]:

$$L_{Q_r}(t = t_j) = \gamma \sum_i^{n_b} Q_{r,i} H_{w,i} \tag{3.8}$$

being $Q_{r,i}$ the flowrate exiting from the bucket i at $t = t_j$, whose related head is $H_{w,i}$, and n_b is the number of the buckets contributing to the outflow.

The flow rate $Q_{r,i}$ can be expressed by [35]:

$$Q_{r,i} = \frac{V(\theta_i, \omega) - V(\theta_i + d\theta, \omega)}{d\theta/\omega} = -\omega \frac{\partial V}{\partial \theta}\bigg|_{\theta = \theta_i} \tag{3.9}$$

where $V(\theta_i, \omega)$ is the maximum water volume each bucket i can contain in its position $\theta = \theta_i$ for a certain angular speed ω.

The emptying process starts at the position $\theta = \theta_e$ where $V(\theta, \omega) = V_{in}$, being $V(\theta, \omega)$ the maximum water volume the bucket can contain, and V_{in} the water volume that entered the bucket in the filling process, all the buckets beyond the position θ_e contribute to L_{Q_r}. $V = V(\theta, \omega)$ depends on the geometric shape of the blades and decreases when θ and ω increases [35]. The volume V_{in} can be expressed by [23]:

$$V_{in} = Q\frac{\beta}{\omega} \tag{3.10}$$

Quaranta and Revelli [35] investigated two scenarios: initially, the effect of the centrifugal force was neglected, and later the centrifugal force was taken into account. In the first scenario, the maximum water volume V is represented by $V_s = V_s(\theta)$, and it depends only on the buckets' geometry and their position θ, being independent of ω. $V_s = V_s(\theta)$ is a characteristic parameter of the overshot water wheel [35].

If the centrifugal force is considered, the maximum water volume is $V = V(\theta, \omega) < V_s(\theta)$ due to the water profile's inclination inside the buckets. The water surface at each point is perpendicular to the total acting force $\vec{F}_t = \vec{F}_c + \vec{F}_g$, where $\vec{F}_c = \omega^2 e$ is the centrifugal acceleration (force for unit mass) and $\vec{F}_g = \vec{g}$ the gravity acceleration, being e the distance between each point of the water surface in the buckets and the wheel rotational axle (m) [35]. For simplicity, considering the water profile to be linear and the mean distance $e = \overline{e}$, V can be calculated assuming that V_{in} reduces by $V_l \approx 1/2 \cdot w h_o^2 \sin\alpha$, being $h_o = h_o(\theta)$ the maximum horizontal length of the water surface inside the buckets (m), and $\sin\alpha = F_c \sin\theta / F_t$, where $\alpha = \alpha(\theta, \omega)$ is the inclination of the water surface due to the effect of the centrifugal force and w is the width of the buckets [35]. The volume V can then be expressed as the difference between V_s and V_l, being a function of θ and ω $(V(\theta, \omega) = V_s - V_l)$.

Chapter 4

Design and Modelling of the Overshot Water Wheel

This chapter presents the investigated water wheel design, considering the characteristics of an existing water wheel and the criteria presented in the previous chapter. Additionally, the developed mathematical modelling of the water wheel is described, which is necessary to calculate the power losses of the wheel through the theoretical methods presented in Chapter 3. The design, modelling and the power losses calculations allow the analysis of the water wheel's behavior and the design of the grid-connected pico-hydropower system in its entirety, as it will be presented in the next chapter.

4.1 Modelling of the Water Wheel

For the proposed system design, the first step was to determine the characteristics of the water wheel. Some of the values used were determined based on a water wheel built for the Castrelos' Aquaculture Center, as part of the ongoing project BIOURB NATUR of the ESTiG, at IPB.

The site's hydraulic characteristics considered for the water wheel's design are: $H_{net} = 2.3$ m, and $Q_{net} = 0.025$ m^3/s. The wheel's diameter is $D = 2$ m, the

inner and outer radius of the wheel are $R_i = 0.8$ m and $R_o = 1$ m, respectively. The bucket depth (in the radial direction) is $d = 0.2$ m, the number of buckets is equal to $n = 20$, the angular distance between two buckets/blades is $\beta = 18°$, and the wheel width is $w = 0.26$ m. Figure 4.1 illustrates the water wheel. Based on these values, a filling ratio of 0.45 at a rotational speed of $N = 11$ rpm was chosen. The critical rotational speed was identified as $N_{cr} = 22$ rpm.
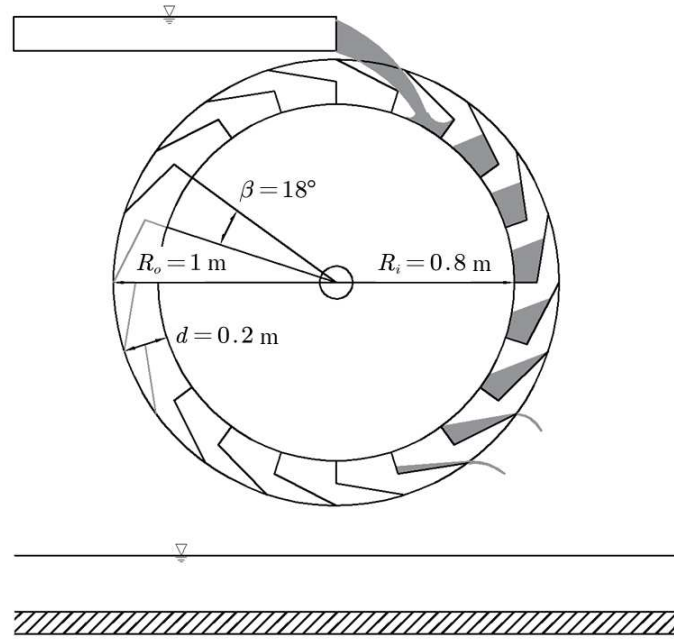
Figure 4.1 Representation of the water wheel.

As mentioned in section 3.2, the blade profile selected was the one with a flat bottom based on the historical literature. Figure 4.2 shows the designed bucket, where: $b = 0.1$ m is the bottom of the bucket, $s = 0.313$ m is the side of the bucket, and $\sigma = 99°$ is the angle formed between b and s. For the system analysis, it was necessary to calculate the maximum volume of the bucket at the top of the wheel and to obtain a mathematical model describing the maximum water volume that each bucket can hold according to the rotation angle θ.
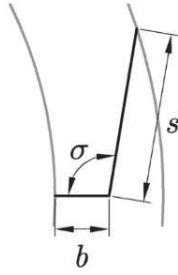
Figure 4.2 Designed bucket.

4.1.1 Maximum volume of the bucket at the top of the wheel

The maximum volume of the bucket at the top of the wheel was calculated, considering the one shown in Figure 4.3. The arc lengths A_o and A_i were approximated by the line segments $A_o{}'$ and $A_i{}'$, respectively. The bucket section was divided into three areas, equivalent to two triangles and a trapezoid, as shown in Figure 4.4.
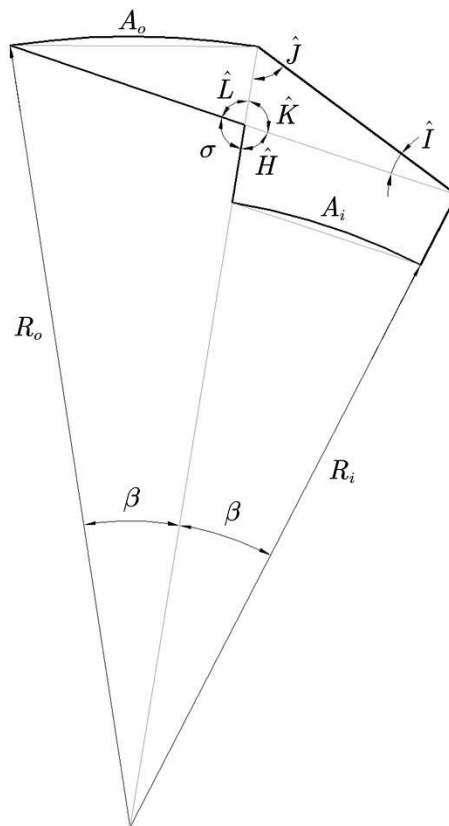
Figure 4.3 Bucket configuration at the top of the wheel.
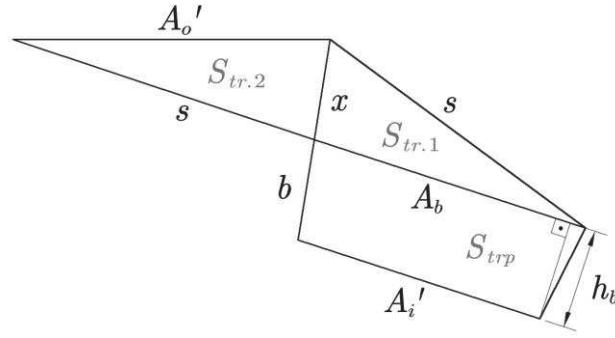
Figure 4.4 Equivalent area of the bucket at the top of the wheel.

A_o', A_i' and A_b can be determined by the law of cosines and are equal to:

$$A_o' = \sqrt{2R_o^2(1-\cos\beta)} \tag{4.1}$$

$$A_i' = \sqrt{2R_i^2(1-\cos\beta)} \tag{4.2}$$

$$A_b = \sqrt{2(R_i+b)^2(1-\cos\beta)} \tag{4.3}$$

The angle $\hat{H}$ and the height h_b, necessary for the calculation of the trapezoid area are:

$$\hat{H} = \frac{180° - \beta}{2} \tag{4.4}$$

$$h_b = b\sin\hat{H} \tag{4.5}$$

The Equation (4.6) expresses the trapezoid area:

$$S_{trap} = \frac{(A_b + A_i')h_b}{2} \tag{4.6}$$

The angle $\hat{I}$ and the triangle area $S_{tr.1}$ are expressed by:

$$\hat{I} = \sigma - \hat{H} \tag{4.7}$$

$$S_{tr.1} = \frac{sA_b\sin\hat{I}}{2} \tag{4.8}$$

The values of x, $\hat{K}$ and $\hat{L}$ needed to determine the triangle area $S_{tr.2}$ are obtained by:

$$x = \sqrt{A_b^2 + s^2 - 2A_b s \cos \hat{I}} \tag{4.9}$$

$$\hat{K} = \arcsin\left(\frac{s \sin \hat{I}}{x}\right) \tag{4.10}$$

$$\hat{L} = 360° - \hat{K} - \hat{H} - \sigma \tag{4.11}$$

The Equation (4.12) represents the area $S_{tr.2}$:

$$S_{tr.2} = \frac{sx \sin \hat{L}}{2} \tag{4.12}$$

Finally, the Equation (4.13) expresses the whole section of the bucket:

$$S_{top} = S_{trp} + S_{tr.1} + S_{tr.2} \tag{4.13}$$

and the Equation (4.14) the total volume:

$$V_{top} = w S_{top} \tag{4.14}$$

The Equation (4.14) is necessary to determinate the wheel's width, for a given rotational speed in order to satisfy the desired filling ratio, obtained by:

$$\text{filling ratio} = \frac{V_{in}}{V_{top}} \tag{4.15}$$

V_{in} is the water volume that entered the bucket in the filling process, described in the previous chapter by Equation (3.10):

$$V_{in} = Q \frac{\beta}{\omega} \tag{3.10}$$

As the water wheel investigated in this work was designed based on an existing overshot water wheel, its width was already determined. Therefore, the design process was conducted differently. Instead, the wheel's rotational speed was calculated for the given width in order to satisfy the desired filling ratio.

4.1.2 Maximum water volume inside the buckets

For the calculation of the maximum water volume that each bucket can hold as a function of the rotation angle θ, two moments were identified: in the first, the bucket profile includes the circumference of radius R_i, and in the second, the bucket profile does not include such circumference, being formed only by the bucket blade, as shown in Figure 4.5.
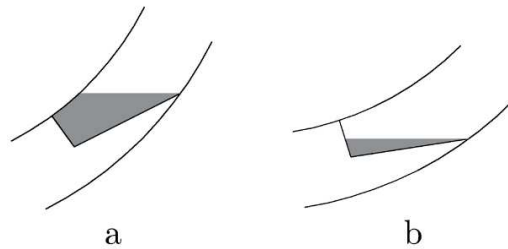
Figure 4.5 Maximum volume of water inside the bucket when: (a) including the internal circumference, (b) formed only by the bucket blade.

For the first moment, the analysis was made considering the bucket shown in Figure 4.6. Being $\phi = \theta - 90°$, h_o is the maximum horizontal distance of the water surface inside the bucket. Initially, the bucket profile section was divided into two areas, namely S_1 and S_2. The arc length formed by the internal circumference (of radius R_i) was approximated by the line segment l', making S_1 and S_2 equivalent to two triangles, as presented in Figure 4.7.
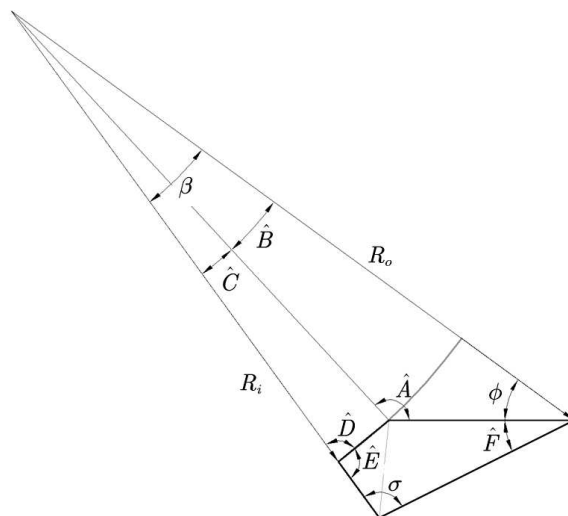
Figure 4.6 Bucket (a) configuration.
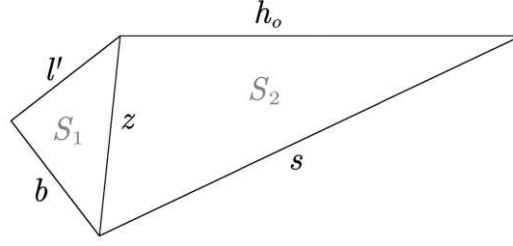
Figure 4.7 Equivalent area of the bucket (a).

By the law of sines, it was possible to determine h_o as follows:

$$\frac{R_o}{\sin \hat{A}} = \frac{R_i}{\sin \phi} = \frac{h_o}{\sin \hat{B}} \tag{4.16}$$

$$\hat{A} = \left(-\arcsin\left(\frac{R_o \sin \phi}{R_i}\right)\right) \tag{4.17}$$

$$\hat{B} = 180° - \hat{A} - \phi \tag{4.18}$$

$$h_o = \frac{R_i}{\sin \phi} \cdot \sin \hat{B} \tag{4.19}$$

making the necessary substitutions and simplifications h_o is expressed by Equation (4.20):

$$h_o = -R_i \sec\theta \cos\left(\theta + \arcsin\left(\frac{R_o}{R_i}\cos\theta\right)\right) \tag{4.20}$$

Being l' the base of the R_i sided isosceles triangle, spaced by the angle $\hat{C}$, l' can be obtained by:

$$(l')^2 = 2(R_i)^2 - 2(R_i)^2 \cos\hat{C} \tag{4.21}$$

$$l' = \sqrt{2(R_i)^2 \cdot \left(1 - \cos\hat{C}\right)} \tag{4.22}$$

where $\hat{C} = \beta - \hat{B}$. The angles $\hat{D}$, $\hat{E}$ and $\hat{F}$ necessary for the calculation of S_1 and S_2 are:

$$\hat{D} = \frac{180° - \hat{C}}{2} \tag{4.23}$$

$$\hat{E} = 180° - \hat{D} \tag{4.24}$$

$$\hat{F} = 180° - \beta - \sigma - \phi \tag{4.25}$$

The triangles area S_1 and S_2 can be expressed by:

$$S_1 = \frac{\sin \hat{E} \cdot l' \cdot b}{2} \tag{4.26}$$

$$S_2 = \frac{\sin \hat{F} \cdot h_o \cdot s}{2} \tag{4.27}$$

making the appropriate substitutions and simplifications to the Equations (4.26) and (4.27), the Equations (4.28) and (4.29) are obtained:

$$S_1 = \frac{b}{2} \sin\left(\frac{1}{2}\left(90° + \beta + \theta + \arcsin\left(\frac{R_o}{R_i}\cos\theta\right)\right)\right)$$
$$\cdot \sqrt{\left(2(R_i)^2\left(1 - \cos\left(\beta - 90° + \theta + \arcsin\left(\frac{R_o}{R_i}\cos\theta\right)\right)\right)\right)} \tag{4.28}$$

$$S_2 = \sin\left(270° - \beta - \sigma - \theta\right)\left(-R_i \sec\theta \cos\left(\theta + \arcsin\left(\frac{R_o}{R_i}\cos\theta\right)\right)\right) \tag{4.29}$$

The total active area of the bucket is $S_{t.a} = S_1 + S_2$, and the total volume of the bucket is obtained by multiplying it by the wheel width, represented in Equation (4.30):

$$V_a = w S_{t.a} \tag{4.30}$$

For the second moment, where the bucket profile does not include the circumference of radius R_i, it was considered the bucket presented in Figure 4.8. The active area of the bucket is S_3, as shown in Figure 4.9.
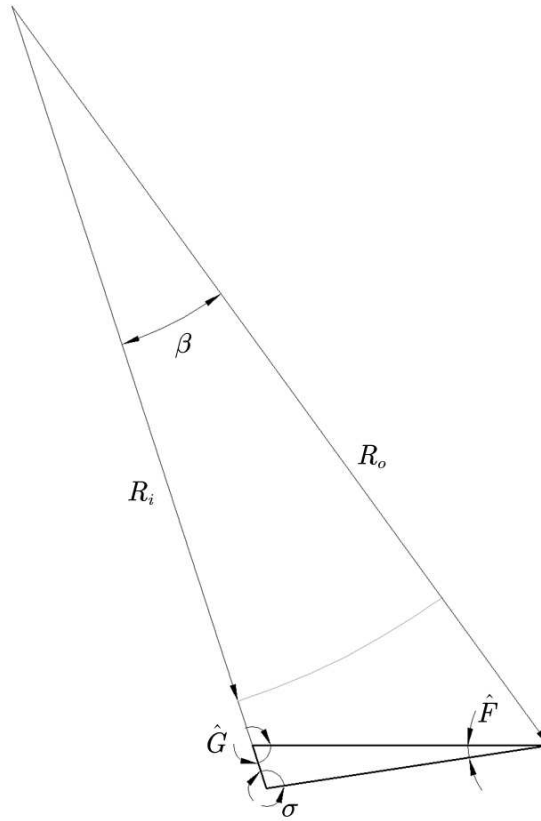
Figure 4.8 Bucket (b) configuration.

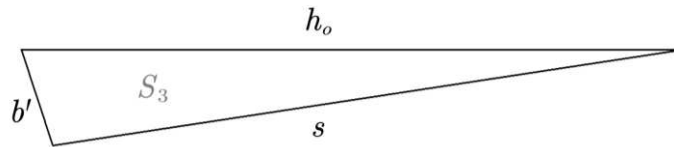Figure 4.9 Equivalent area of the bucket (b).

Knowing that the sum of the internal angles of any triangle is equal to 180°, $\hat{G}$ can be obtained by:

$$\hat{G} = 180° - \sigma - \hat{F} \tag{4.31}$$

By the law of sines, it is possible to obtain h_o:

$$\frac{b'}{\sin \hat{F}} = \frac{h_o}{\sin \sigma} = \frac{s}{\sin \hat{G}} \tag{4.32}$$

$$h_o = \frac{s}{\sin \hat{G}} \cdot \sin \sigma \tag{4.33}$$

making the proper substitutions and simplifications to Equation (4.33), h_o is expressed by Equation (4.34):

$$h_o = s \cdot \frac{\sin\sigma}{\sin\left(\beta + \theta - 90°\right)} \tag{4.34}$$

The active area of the bucket (S_3) is equal to:

$$S_3 = \frac{\sin\hat{F} \cdot h_o \cdot s}{2} \tag{4.35}$$

$$S_3 = \frac{s^2}{2} \cdot \frac{\sin\sigma\cos\left(\theta + \sigma + \beta\right)}{\cos\left(\theta + \beta\right)} \tag{4.36}$$

Finally, Equation (4.37) expresses the active volume of the bucket:

$$V_b = wS_3 \tag{4.37}$$

A scale model of the wheel was created in the software AutoCAD. A series of tests comparing the values calculated by the previous equations and the ones obtained by the graphic method were made to validate them.

Knowing the equations of h_o for both scenarios identified, it was possible to include the centrifugal force's effect into consideration, using the equation $V_l \approx 1/2 \cdot wh_o^2\sin\alpha$ presented in Chapter 3.

The Equations (4.30) and (4.37), including the centrifugal force's effect, are necessary to calculate the flowrate lost during rotation $(Q_{r,i})$, presented in the previous chapter and expressed by the Equation (3.9):

$$Q_{r,i} = \frac{V\left(\theta_i,\omega\right) - V\left(\theta_i + d\theta,\omega\right)}{d\theta/\omega} = -\omega\frac{\partial V}{\partial\theta}\bigg|_{\theta=\theta_i} \tag{3.9}$$

4.2 Following procedures

The wheel efficiency was measured for various values of rotational speed. This range's initial speed was determined as to when the volume of water entering the

wheel (V_{in}) is equal to the maximum volume of water that the bucket in the position $\theta = 90°$ can contain, for simplicity of analysis. Taking into consideration the above mentioned, the head of water of each bucket (concerning the blade tip) was calculated by the Equation (4.38):

$$H_{w,i} = R_o - R_o \sin \phi + H_D \tag{4.38}$$

With the values and equations described, it was possible to apply the power losses estimation model developed by Quaranta and Revelli [35] presented in section 3.3. The calculations were performed using the software MATLAB.

The calculated values were recorded and converted into a graph expressing the wheel's output power for different speed values. With this data, it was possible to analyze the water wheel's behavior within an operational range and choose the appropriate electrical generator and PV inverter, based on the approach described by Leite et al. [16] presented in Section 2.6.

For comparison, the output power of the wheel was also calculated using the model described by Church [30]:

$$P_{out,C} = \rho g Q_{net} \left[\frac{(v \cos \lambda - u) u}{g} + h_2 + \delta h_3 \right] \tag{4.39}$$

Where λ is the angle between $\vec{v}$ and $\vec{u}$ at the point of impact of the water jet in the bucket, h_2 is the distance between the water surface in the first bucket to be filled and the water surface in the bucket just before the emptying process begins, h_3 is the distance between the last bucket described and the tip of the bucket that immediately emptied, and $\delta = 0.5$ is an error coefficient introduced by Church [30].

Chapter 5

Results and Analysis

This chapter presents the results obtained based on the theoretical models and procedures described in Chapter 4. Additionally, it presents the analysis and discussions about the proposed grid-connected pico-hydro system.

5.1 Theoretical results

From the procedures described in Chapter 4, a curve of the water wheel's output power (P_{out}) as a function of the rotational speed (N) was obtained, illustrated in Figure 5.1.
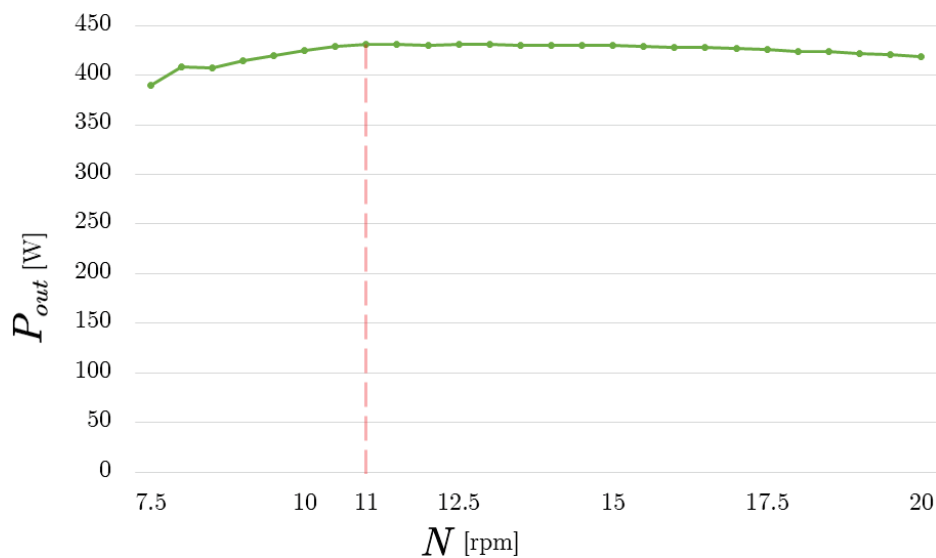
Figure 5.1 Output power P_{out} versus rotational speed N.

This curve describes the water wheel's expected behavior coherently with what the literature presents [13], [23], [35]. The low output power for the initial speed values can be attributed to the fact that the buckets' water volume is higher for lower speed values. Therefore, during rotation, the emptying process starts earlier, even if the centrifugal force's effect is less than for higher speeds. Additionally, the water jet's relative speed at the jet's impact point is higher, making the impact losses (L_{imp}) more significant. It is also observed that the maximum power value occurs at the speed value for which the wheel was designed $(N = 11$ rpm$)$, which is within the optimal range of the filling ratio $(0.3 - 0.5)$. The reduction of the output power with the increase of the rotational speed occurs due to the rise of the centrifugal force's effect, causing the emptying process to start earlier.

It is important to note that the calculations were performed within the optimal operating range of overshot water wheels $(N < N_{cr})$ when volumetric losses at the top of the wheel are negligible. It can also be highlighted that the wheel's output power varies slightly for a wide range of speed values, with an almost constant efficiency of $\simeq 76\%$, as shown in Figure 5.2.
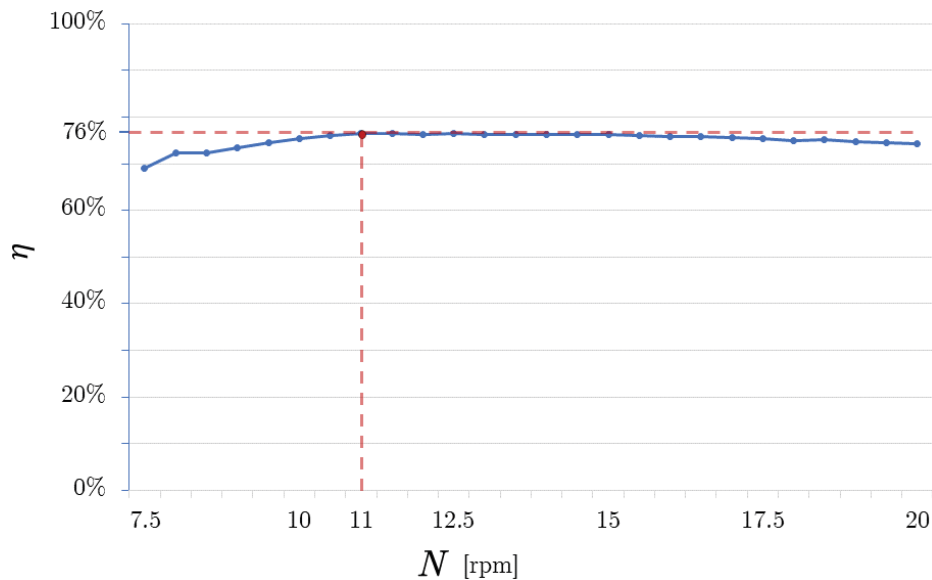
Figure 5.2 Efficiency η versus rotational speed N.

Table 5.1 shows the maximum output power and efficiency values obtained by the method developed by Quaranta and Revelli [35] and those obtained by the one described by Church [30]. The discrepancy between the results is as expected since the method proposed by Church is a simplified method for estimating the efficiency and considers that the impact of the water jet in the bucket contributes to the power generation and is not a loss of the system, contrary to the one proposed by Quaranta and Revelli.

Table 5.1 Maximum values of P_{out} and η by the methods of Quaranta and Revelli and Church.

Authors	P_{out} (W)	η (%)
Quaranta and Revelli	431.06	76
Church	478.81	85

The curve illustrated and the values presented so far refer only to the mechanical generation's values and do not include the electric generator's losses.

5.2 Analysis of the electricity generation system with grid connection

With the data obtained, it was possible to design a suitable electrical generation system with grid connection, according to the topology proposed in [16] and presented in section 2.6. Figure 5.3 shows the topology for the proposed system. For this system, the PMSG with the characteristics shown in Table 5.2 and the PV micro-inverters presented in Table 5.3 were considered. To couple the investigated water wheel and the chosen generator, there is a need for a gearbox; a suitable ratio is $1:15$. Considering the efficiency of the PMSG, the maximum output power of the system is $P_{out} = 366.41$ W, and the global efficiency is $\eta = 65\%$.
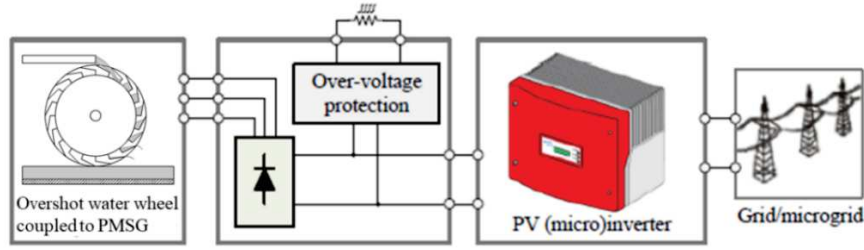
Figure 5.3 Topology for the proposed system, adapted from [16].

Table 5.2 PMSG technical characteristics [57].

Generator	Speed (rpm)	$\mathbf{V}_{DC}$ (V)	I_{DC} (A)	P_{DC} (W)	η (%)
TGET320	200	56	8.9	500	85

Table 5.3 PV micro-inverters technical characteristics [58]–[60].

Inverter	$P_{DC\max}$ (W)	$I_{DC\max}$ (A)	$\mathbf{V}_{DCrange}$ (V)	$\mathbf{V}_{MPPrange}$ (V)	$\mathbf{V}_{PVstart}$ (V)
INV500-90	500	11	40-90	40-80	40
MI-800N	800	12.5	16-60	34-48	22
SG450HS	450	12.5	30-70	36-60	30

The rated voltage of the PMSG is within the input voltage range of all selected PV micro-inverters. As the generator's no-load voltage is unknown, the system must be designed with an over-voltage protection circuit for safety reasons. The voltage allowed by it must be less than the maximum input voltage of the desired PV-micro-inverter. The maximum power expected from the system and the generator current also respect the micro-inverters' specifications.

5.3 Discussion

It was possible to design a grid-connected pico-hydropower system, based on the generator and PV micro-inverters' technical characteristics, respecting the integration requirements between the described elements (water wheel, PMSG,

and PV micro-inverter). However, the theoretical analysis alone does not provide all the factors that must be considered, such as the PV micro-inverters' MPPT algorithm's dynamics, requiring experimental tests to validate these results. Nevertheless, the process developed, and the results obtained serve as an initial step in designing and comprehending this system.

Additionally, applying existing theoretical models as done in this work can help fill a gap in the bibliography. Since obtaining a curve, like the one illustrated in Figure 5.1, which describes the water wheel's behavior within an operational range, can allow for the emulation of an accurate water wheel model. Such a system is attractive considering that the manufacture of water wheels for experimental tests and the construction of an environment that allows testing it is not always feasible. Besides, a precise emulation would allow a more in-depth analysis of MPPT algorithms' performance when integrated into these systems.

Chapter 6

Conclusions

In this work, the design and analysis of an overshot water wheel were made in the context of a grid-connected pico-hydro system, within the scope of the BIOURB NATUR project. The system design was based on the integration of the water wheel with a PMSG and conventional PV micro-inverters.

The water wheel's design was made following the criteria present in the literature and having as a model a water wheel built for the Castrelos' Aquaculture Center, as part of the ongoing project BIOURB NATUR of the ESTiG, at IPB. The wheel was designed considering a head of 2.3 m and flowrate of 0.025 m^3/s, with a diameter of 2 m, a width of 0.26 m, 20 buckets shaped with a flat-bottom and depth of 0.2 m. Additionally, for the design, a rotational speed of 11 rpm was considered.

The mathematical modelling of the water wheel was made, allowing the application of a theoretical model to estimate its efficiency. Following this, the output power of the water wheel was obtained for different speed values between 7.5 rpm and 20 rpm. The maximum theoretical mechanical output power achieved was 431.06 W at a speed of 11 rpm, corresponding to an efficiency of 76%. The data obtained were computed and converted into a graph describing the water wheel's behavior within an operational range.

Although the experimental validation was no conducted in this work, the results achieved indicate the possibility to design the proposed grid-connected pico-hydro system. For this system, a PMSG with a rated power of 500 W and speed of 300 rpm was considered, being identified the need of a gearbox for the coupling with the water wheel. Considering the PMSG efficiency, the maximum theoretical output power obtained was 366.41 W with a global efficiency of 65%. For the grid interface, the characteristics of three conventional PV micro-inverters were analyzed, namely INV500-90, MI-800N, and SG450HS, wherein all the micro-inverters respected the compatibility criteria for the integration with the PMSG. However, it is necessary to perform experimental tests to analyze the compatibility between the micro-inverters MPPT's algorithm dynamics and the proposed pico-hydro system. Additionally, this interface with the grid indicates the possibility of the water wheel to operate at variable speed and in different hydraulic conditions (head and flowrate).

It is worth mentioning that the connection with the grid using conventional PV micro-inverters can facilitate the dissemination of these systems since PV micro-inverters are off-the-shelf solutions with a high level of technological maturity. Also, the studies developed in the realization of this work emphasize the emerging potential of pico-hydro systems to exploit the energetic potential in rivers and watercourses, especially in rural and remote communities.

6.1 Future work

In the planning of this work, initially, practical and experimental activities were projected to be carried out, which included:

- Experimental validation of the results obtained and the analysis of the micro-inverters MPPT's algorithm dynamics through the emulation of the proposed system, based on the graph that describes the behavior of the water wheel within an operational range;

- Analysis and comparison with the water wheel that is going to be installed in the Castrelos' Aquaculture Center, by the end of November 2020.

However, due to the pandemic related to COVID-19, these activities were compromised. Therefore, it is suggested that future works address them.

References

[1]   International Energy Agency (IEA), "World Energy Outlook 2018 -
        Renewables," *Flagsh. Rep.*, 2018, [Online]. Available:
        https://www.iea.org/reports/world-energy-outlook-
        2018/renewables#abstract.

[2]   EU, "Directive (EU) 2018/2001 of the European Parliament and of the
        Council on the promotion of the use of energy from renewable sources,"
        Off. J. Eur. Union, vol. 2018, no. L 328, pp. 82–209, 2018, [Online].
        Available: https://eur-lex.europa.eu/legal-
        content/EN/TXT/PDF/?uri=CELEX:32018L2001&from=EN.

[3]   European Parliament, "Directive 2018/2002/EU amending Directive
        2012/27/EU on Energy Efficiency," *Off. J. Eur. Union*, vol. 328, no.
        November, pp. 210–230, 2018, [Online]. Available: https://eur-
        lex.europa.eu/legal-
        content/EN/TXT/PDF/?uri=CELEX:32018L2002&from=EN.

[4]   U. Nations, "Transforming Our World: The 2030 Agenda for Sustainable
        Development," *A New Era Glob. Heal.*, 2018, doi:
        10.1891/9780826190123.ap02.

[5]   BP, "Statistical Review of World Energy 2020," 2020. [Online]. Available:
        https://www.bp.com/content/dam/bp/business-
        sites/en/global/corporate/pdfs/energy-economics/statistical-review/bp-
        stats-review-2020-full-report.pdf.

[6]   I. Kougias, *Hydropower Technology Development Report 2018*, no.
        November. 2019.

[7]   CanmetENERGY, "Emerging Hydropower Technologies R&D in Canada:
        A Strategy for 2007-2011," 2007. [Online]. Available:

https://www.nrcan.gc.ca/sites/www.nrcan.gc.ca/files/canmetenergy/files/EmergingHydroPower_2007_2011.pdf.

[8]   K. Bódis, F. Monforti, and S. Szabó, "Could Europe have more mini hydro sites? A suitability analysis based on continentally harmonized geographical and hydrological data," *Renew. Sustain. Energy Rev.*, vol. 37, pp. 794–808, 2014, doi: 10.1016/j.rser.2014.05.071.

[9]   A. A. Williams and R. Simpson, "Pico hydro - Reducing technical risks for rural electrification," *Renew. Energy*, vol. 34, no. 8, pp. 1986–1991, 2009, doi: 10.1016/j.renene.2008.12.011.

[10]   I. Kougias *et al.*, "Analysis of emerging technologies in the hydropower sector," *Renew. Sustain. Energy Rev.*, vol. 113, no. July, 2019, doi: 10.1016/j.rser.2019.109257.

[11]   UNIDO - United Nations Industrial Development Organization, "World Small Hydropower Development Report 2019," p. 69, 2019, [Online]. Available: www.smallhydroworld.org.

[12]   E. Quaranta and R. Revelli, "Gravity water wheels as a micro hydropower energy source: A review based on historic data, design methods, efficiencies and modern optimizations," *Renew. Sustain. Energy Rev.*, vol. 97, no. August, pp. 414–427, 2018, doi: 10.1016/j.rser.2018.08.033.

[13]   G. Müller and K. Kauppert, "Performance characteristics of water wheels," *J. Hydraul. Res.*, vol. 42, no. 5, pp. 451–460, 2004, doi: 10.1080/00221686.2004.9641215.

[14]   I. de C. Dalmarco, P. H. A. de Araujo, A. V. T. Leite, L. M. C. Queijo, and L. E. M. Lima, "Prototyping a horizontal water wheel for electricity generation in a small museum: the House of Silk," *Ciudad. Intel. Total. Integr. Efic. y Sostenibles*, no. March 2020, pp. 809–814, 2018, [Online]. Available: https://repository.usc.edu.co/handle/20.500.12421/375.

[15]   L. G. A. Figueiredo, W. Maidana, and V. Leite, "Implementation of a

Smart Microgrid in a Small Museum: The Silk House," 2020, pp. 121–134.

[16]   V. Leite, J. Couto, A. Ferreira, and J. Batista, "A practical approach for
       grid-connected pico-hydro systems using conventional photovoltaic
       inverters," *2016 IEEE Int. Energy Conf. ENERGYCON 2016*, 2016, doi:
       10.1109/ENERGYCON.2016.7513911.

[17]   G. M. Ribeiro, W. Maidana, V. Leite, and A. Ferreira, "Grid Connection
       Approach for Very Small-Scale Pico-Hydro Systems Using PV
       Microinverters," *IECON Proc. (Industrial Electron. Conf.*, vol. 2019-
       Octob, pp. 2372–2376, 2019, doi: 10.1109/IECON.2019.8926691.

[18]   V. Leite, A. Ferreira, J. Couto, and J. Batista, "Compatibility analysis of
       grid-connected pico-hydro systems using conventional photovoltaic
       inverters," *2016 18th Eur. Conf. Power Electron. Appl. EPE 2016 ECCE
       Eur.*, 2016, doi: 10.1109/EPE.2016.7695615.

[19]   M. Silva, V. Leite, D. Roman, P. Araújo, W. Maidana, and J. Batista,
       "Design of a Microgrid Based on Renewable Energy Sources for an
       Aquaculture Centre," in *I Ibero-American Congress of Smart Cities
       (ICSC-CITIES 2018)*, 2018, pp. 579–591.

[20]   M. Silva *et al.*, "Designing Innovative Home Energy Systems for Smart
       Cities: The SilkHouse Project," in *I Ibero-American Congress of Smart
       Cities (ICSC-CITIES 2018)*, 2018, pp. 898–914.

[21]   IRENA, "Renewable Energy Technologies: Cost Analysis Series,
       Hydropower," *Int. Renew. Energy Agency*, vol. 1, no. 3/5, p. 44, 2012,
       [Online]. Available:
       http://www.irena.org/documentdownloads/publications/re_technologies_
       cost_analysis-hydropower.pdf.

[22]   A. Harvey, *Micro-Hydro Design Manual: A Guide to Small-Scale Water
       Power Schemes*. Intermediate Technology Publications, 1993.

[23]   E. Quaranta, "Investigation and optimization of the performance of

53

gravity water wheels," Politecnico di Torino, 2017.

[24] P. J. Pritchard, *Fox and McDonald's Introduction to Fluid Mechanics*, 8th ed. John Wiley & Sons, 2011.

[25] L. Barelli, L. Liucci, A. Ottaviano, and D. Valigi, "Mini-hydro: A design approach in case of torrential rivers," *Energy*, vol. 58, pp. 695–706, 2013, doi: 10.1016/j.energy.2013.06.038.

[26] S. J. Williamson, B. H. Stark, and J. D. Booker, "Low head pico hydro turbine selection using a multi-criteria analysis," *Renew. Energy*, vol. 61, pp. 43–50, 2014, doi: 10.1016/j.renene.2012.06.020.

[27] S. Bozhinova, V. Hecht, D. Kisliakov, G. Muller, and S. Schneider, "Hydropower converters with head differences below 2.5m," *Proc. Inst. Civ. Eng. Energy*, vol. 166, no. 3, pp. 107–119, 2013, doi: 10.1680/ener.11.00037.

[28] O. Paish, "Micro-hydropower: Status and prospects," *Proc. Inst. Mech. Eng. Part A J. Power Energy*, vol. 216, no. 1, pp. 31–40, Feb. 2002, doi: 10.1243/095765002760024827.

[29] F. C. Lea, *Hydraulics for Engineers and Engineering Students*. Edward Arnold, 1911.

[30] I. P. Church, *Hydraulic Motors: With Related Subjects, Including Centrifugal Pumps, Pipes, and Open Channels, Designed as a Text-Book for Engineering Schools*. John Wiley & Sons, 1905.

[31] T. Pujol and L. Montoro, "High hydraulic performance in horizontal waterwheels," *Renew. Energy*, vol. 35, no. 11, pp. 2543–2551, 2010, doi: 10.1016/j.renene.2010.03.025.

[32] T. Pujol, J. Solà, L. Montoro, and M. Pelegrí, "Hydraulic performance of an ancient Spanish watermill," *Renew. Energy*, vol. 35, no. 2, pp. 387–396, 2010, doi: 10.1016/j.renene.2009.03.033.

[33] R. E. Horton, "Turbine Water-Wheel Tests and Power Tables," p. 138, 1906.

[34] G. Müller, S. Denchfield, R. Marth, and B. Shelmerdine, "Stream wheels for applications in shallow and deep water," *32nd IAHR Conf. 2007, Venice, Italy, 01 - 06 Jul 2007.*, no. 1, pp. 1–9, 2007.

[35] E. Quaranta and R. Revelli, "Output power and power losses estimation for an overshot water wheel," *Renew. Energy*, vol. 83, pp. 979–987, 2015, doi: 10.1016/j.renene.2015.05.018.

[36] E. Quaranta and R. Revelli, "Performance characteristics, power losses and mechanical power estimation for a breastshot water wheel," *Energy*, vol. 87, pp. 315–325, 2015, doi: 10.1016/j.energy.2015.04.079.

[37] D. A. Howey, "Axial Flux Permanent Magnet Generator for Pico-Hydropower," in *EWB-UK Research Conference*, 2009.

[38] A. Dietz, A. Groeger, and C. Klingler, "Efficiency improvement of small hydroelectric power stations with a permanent-magnet synchronous generator," *1st Int. Electr. Drives Prod. Conf. 2011, EDPC-2011 - Proc.*, pp. 93–100, 2011, doi: 10.1109/EDPC.2011.6085557.

[39] N. P. A. Smith, "Induction Generators for Stand-Alone Micro-Hydro Systems," *Proc. IEEE Int. Conf. Power Electron. Drives Energy Syst. Ind. Growth, PEDES*, vol. 2, pp. 669–673, 1996, doi: 10.1109/pedes.1996.535860.

[40] E. Hau, *Wind Turbines: Fundamentals, Technologies, Application, Economics*, 2nd ed. Springer, 2006.

[41] S. D. Umans, *Máquinas Elétricas de Fitzgerald e Kingsley*, 7th ed. AMGH, 2014.

[42] F. H. Schwartz and M. Shahidehpour, "Small Hydro as Green Power," *2006 IEEE EIC Clim. Chang. Technol. Conf. EICCCC 2006*, pp. 1–8,

2006, doi: 10.1109/EICCCC.2006.277197.

[43] S. J. Chapman, *Fundamentos de Máquinas Elétricas*, 5th ed. AMGH, 2013.

[44] T. F. Chan and L. L. Lai, "Permanent-magnet machines for distributed power generation: A review," *2007 IEEE Power Eng. Soc. Gen. Meet. PES*, pp. 6–11, 2007, doi: 10.1109/PES.2007.385575.

[45] International Energy Agency (IEA), "Distributed Generation in Liberalised Electricity Markets," *Int. Energy Agency*, p. 124, 2002, doi: 10.1787/9789264175976-en.

[46] T. Ackermann, G. Andersson, and L. Söder, "Distributed generation: A definition," *Electr. Power Syst. Res.*, vol. 57, no. 3, pp. 195–204, 2001, doi: 10.1016/S0378-7796(01)00101-8.

[47] G. Pepermans, J. Driesen, D. Haeseldonckx, R. Belmans, and W. D'haeseleer, "Distributed generation: Definition, benefits and issues," *Energy Policy*, vol. 33, no. 6, pp. 787–798, 2005, doi: 10.1016/j.enpol.2003.10.004.

[48] P. Dondi, D. Bayoumi, C. Haederli, D. Julian, and M. Suter, "Network integration of distributed power generation," *J. Power Sources*, vol. 106, no. 1–2, pp. 1–9, 2002, doi: 10.1016/S0378-7753(01)01031-X.

[49] International Renewable Energy Agency (IRENA), "Innovation Landscape Brief: Renewable Mini-Grids," 2019.

[50] S. J. Williamson, A. Griffo, B. H. Stark, and J. D. Booker, "Control of parallel single-phase inverters in a low-head pico-hydro off-grid network," *IECON Proc. (Industrial Electron. Conf.*, pp. 1571–1576, 2013, doi: 10.1109/IECON.2013.6699367.

[51] D. P. Kaundinya, P. Balachandra, and N. H. Ravindranath, "Grid-connected versus stand-alone energy systems for decentralized power-A

review of literature," *Renew. Sustain. Energy Rev.*, vol. 13, no. 8, pp. 2041–2050, 2009, doi: 10.1016/j.rser.2009.02.002.

[52] A. Hirsch, Y. Parag, and J. Guerrero, "Microgrids: A review of technologies, key drivers, and outstanding issues," *Renew. Sustain. Energy Rev.*, vol. 90, no. March, pp. 402–411, 2018, doi: 10.1016/j.rser.2018.03.040.

[53] A. M. A. Haidar, M. F. M. Senan, A. Noman, and T. Radman, "Utilization of pico hydro generation in domestic and commercial loads," *Renew. Sustain. Energy Rev.*, vol. 16, no. 1, pp. 518–524, 2012, doi: 10.1016/j.rser.2011.08.017.

[54] W. G. Ovens, "A Design Manual for Water Wheels," *Vita Publ.*, p. 84, 1977.

[55] C. R. Weidner, *Theory and Test of an Overshot Water Wheel*. University of Wisconsin, 1913.

[56] M. Denny, "The efficiency of overshot and undershot waterwheels," *Eur. J. Phys.*, vol. 25, no. 2, pp. 193–202, 2004, doi: 10.1088/0143-0807/25/2/006.

[57] Hefei Top Grand Energy Technology Co. Ltd, "Product Detail TGET320-0.5KW-200R." http://www.china-topgrand.com/product_new/.

[58] AEconversion GmbH & Co. KG, "Datasheet INV500-90." 2019, [Online]. Available: http://www.aeconversion.de/files/Datasheet_INV500-90_50Hz_60Hz_EN.pdf.

[59] Hoymiles Converter Technology Co. Ltd, "Datasheet MI-600N/700N/800N." 2019, [Online]. Available: https://www.hoymiles.com/files/a7e78bd0-e891-490e-9475-39b3574f8a64.pdf.

[60] New Energy Technology Co. Ltd., "SG450 Series Datasheet." 2019,

[Online]. Available:

http://www.newenergytek.com/download/datasheet/NETek_SG450_Dat

asheet_EN_V1.8_2019_06_29.pdf.